INTERNATIONAL JOURNAL OF MATHEMATICAL MODELS AND METHODS IN APPLIED SCIENCES
DOI: 10.46300/9101.2022.16.3 Volume 16, 2022

Object Identification by Signal Gain and Correlation

Ching-Liang Su

Department of Industrial Engineering and Technology Management
Da Yeh University
#168, University Road, Dacun, Chang-Hua, 51505, Taiwan
Tel: 886-4-851-1888 ex 4121, Fax: 886-4-851-1270
cls2@mail.dyu.edu.tw

Received: March 15, 2021. Revised: Novemeber 14, 2021. Accepted: December 23, 2021. Published: January 10, 2022.

***Abstract*—In this study, "ring rotation invariant transform" techniques are used to add more salient feature to the original images. The "ring rotation invariant transform" can solve image rotation problem, which transfers a ring signal to several signal vectors in the complex domain, whereby to generate invariant magnitude. Matrix correlation is employed to combine these magnitudes to generate the various discriminators, by which to identify objects. For managing image-shifting problem, one pixel in sample image is compared with surrounding pixels of unknown image. The comparison approaching in this study is by the basis of pixel-to-pixel-comparisons.**

***Keywords*—Object image recognition; moment mapping; matrix correlation; orientation invariant transform.**

I. Introduction

In the past twenty years, researchers have devoted much attention to identify images, which have included: directional histogram equalization [2, 4, 17], binary image stream angle [2, 4, 17], principal component analysis [3, 12], bright indicator [5, 10, 11, 15, 16], Sine component mapping, the IFFT filter, minutia location shape matching [1, 7, 8, 14], fine binary, orientation estimation [6], the Gabor filter [9, 12], feature learning, wavelet transform, singular point detection [12], log polar transform, quad tree, directional detection [2, 4, 17], sub band decomposition, dilate enhancement, feature extraction, ridge tracing, contour following, and u-turn feature. Principal component analysis can identify an object even an object was given various illuminations. It also works even the object was severe distorted. In the real case, after applying this application, a high dimension equation might be generated, which needs to be solved. To solve a high dimension equation is a difficult problem. Control points and line slopes were used in the past as the norm to identify images. However, these features are not always salient. Furthermore, they might be plagued with noise. Therefore, it is very difficult to extract them. Subsequently, it is very difficult to rely on them to identify images. Contour angle histogram locates the edge-curves of the objects. Subsequently, the slopes $tan\theta$ of them can be determined. Later, statistic approaching is used to judge these histograms to determine whether different objects are coming from the same source. Delaunay-tessellation employees some rules to partition object to smaller triangles. These small triangles are used to identify different objects. However this method has the following problems: (1) After several partitions, numerous blocks are generated. The algorithm is unable to record the addresses of beginning and ending points of each individual delimited line of each block. Subsequently, it is difficult to use them to identify different blocks. (2) After several runs of partitions, the algorithm would be very difficult to partition the blocks further. That is because the blocks are too small and they possess too many shapes and, as aforementioned, there are no information about the beginning and ending points of the delimited lines. Congruent transform uses the "image subtraction" technique to find the differences between two objects. For this method to obtain a correct result, this method needs to locate the control points of the object correctly.

Figure 1.1 shows three object images with somewhat different positions and orientations. For comparing them, the following two problems must be solved: (1) image shifting problem, (2) image rotation problem. To solve these two problems, they need to be aligned to the same position and orientation, whereby image comparison can be conducted. This study needs not to move the images, as aforementioned, and the algorithm can recognize them.

In this study, "ring rotation invariant transform" techniques are used to add more salient feature to the original images. It transfers a ring signal to several signal vectors in the complex domain, whereby to generate invariant magnitude, regardless the orientations of the images. Matrix correlation is employed to combine these invariant magnitudes to various discriminators, by which to identify objects. For managing image-shifting problem, one pixel in sample image is compared with surrounding pixels of unknown image. The comparison approaching in this study is by the basis of pixel-to-pixel-comparisons. In the present study, the image-scaling problem is ignored, i.e. the "sample" and "unknown" images possess the same image size. This report consists of four sections. Section 2 shows the mechanism of the "ring rotation invariant transform" and "matrix signal correlation". Section 3 explains the method to manage the image-shifting problem and to perform signal comparison. Section 4 concludes this report.

Figure 1.1: Brush with different orientations.

II. SIGNAL GAINING, MATRIX CORRELATION, AND MOMENT INVARIANT

Equations (2.1-2.5) show the rotation invariant transforms, by which equal quantity can be generated for the ring signals in figures 2.1 and 2.2. Figure 2.1 shows ring-31 circles are used to extract $f(x_k)$ signals in the left and right images, where k varies from 0 to 127; these signals are fed to equation (2.1) to generate the values $F_0(u)$, as represented by 31Ff0. To these two images, 31Ff0 should represent the same value, because equation (2.1) represents the rotation invariant transform; thus, this value is used to identify the images. As this procedure, the left and right images in figure 2.2 using ring-28 circles to generate the $F_0(u)$ signals and they are represented as 28Ff0, which also have the same quantity. Figure 2.3 shows by ring-25, ring-22, ring-19, ring-16, ring-13, and ring-10 to generate 25Ff0, 22Ff0, 19Ff0, 16Ff0, 13Ff0, and 10Ff0 signals, respectively. In the left side of figure 2.4 shows ring-31, 28, 25, and 22 are used to generate 31, 28, 25, and 22Ff0 signals and they are correlated in one matrix to generate the value λ_1, as illustrated in the center. This procedure is applied to the right images and another λ_1 generated; as aforementioned, both should have the same value. These 4 rings are fixed and moved around inside the image to generate various λ_1, as shown in the bottom, whereby they are served as identifiers to identify different images. Figure 2.5 shows ring-19, 16, 13, and 10 are used to generate the 19, 16, 13, and 10Ff0 signals and subsequently λ_2 is generated; applying the aforementioned procedure, various λ_2 can be determined, as shown in the bottom of this figure. Equations (2.6-2.8) show the same procedure to generate λ_4, λ_7, and λ_{10}, as shown in figure 2.6.

The original objects might possess different orientation, as aforementioned in the introduction section; subsequently, the generated lambdas in the top of figure 2.7 have the same subsequence, which have somewhat different orientations; to this study, equations (2.9-2.11) are employed to dealing with this problem.

$$F_0(u) = \| \sum_{k=0}^{127} f(x_k) \| \quad \textbf{(2.1)}$$

$$F_1(u) = \| \sum_{k=0}^{127} f(x_k) e^{-j\cdot 0.28\cdot k} \| \quad \textbf{(2.2)}$$

$$F_2(u) = \| \sum_{k=0}^{127} f(x_k) e^{-j\cdot 0.28\cdot k\cdot 2} \| \quad \textbf{(2.3)}$$

$$F_3(u) = \| \sum_{k=0}^{127} f(x_k) e^{-j\cdot 0.28\cdot k\cdot 3} \| \quad \textbf{(2.4)}$$

$$F_4(u) = \| \sum_{k=0}^{127} f(x_k) e^{-j\cdot 0.28\cdot k\cdot 4} \| \quad \textbf{(2.5)}$$

$$\left.\begin{array}{l} \begin{bmatrix} 19Ff1 & 13Ff1 \\ 16Ff1 & 10Ff1 \end{bmatrix} \rightarrow \lambda_4 \\ F_1(u) = \| \sum_{k=0}^{127} f(x_k) e^{-j\cdot 0.28\cdot k} \| \end{array}\right\} \quad \textbf{(2.6)}$$

$$\left.\begin{array}{l} \begin{bmatrix} 31Ff3 & 25Ff3 \\ 28Ff3 & 22Ff3 \end{bmatrix} \rightarrow \lambda_7 \\ F_3(u) = \| \sum_{k=0}^{127} f(x_k) e^{-j\cdot 0.28\cdot k\cdot 3} \| \end{array}\right\} \quad \textbf{(2.7)}$$

$$\left.\begin{array}{l} \begin{bmatrix} 19Ff4 & 13Ff4 \\ 16Ff4 & 10Ff4 \end{bmatrix} \rightarrow \lambda_{10} \\ F_4(u) = \| \sum_{k=0}^{127} f(x_k) e^{-j\cdot 0.28\cdot k\cdot 4} \| \end{array}\right\} \quad \textbf{(2.8)}$$

$$Var1 = \sum_{j=1}^{N}\sum_{i=1}^{N}(i_{distance})^{2}\cdot Weight_{ij} - \sum_{j=1}^{N}\sum_{i=1}^{N}(j_{distance})^{2}\cdot Weight_{ij} \quad \textbf{(2.9)}$$

$$Var2 = \sum_{j=1}^{N}\sum_{i=1}^{N}2 \cdot i_{distance} \cdot j_{distance} \cdot Weight_{ij} \quad \textbf{(2.10)}$$

$$\theta = \frac{Sin^{-1}\dfrac{\sum_{j=1}^{N}\sum_{i=1}^{N}2\cdot i_{distance}\cdot j_{distance}\cdot Weight_{ij}}{\sqrt{Var2^{2} + Var1^{2}}}}{2} \quad \textbf{(2.11)}$$

Ring 31 **Ring 31**

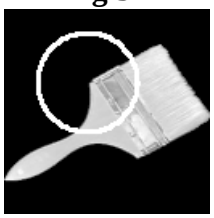


31Ff0 **31Ff0**

$$F_0(u) = \| \sum_{k=0}^{127} f(x_k) \|$$

Figure 2.1: Ring-31 to generate 31Ff0 signals.

Ring-28 **Ring-28**

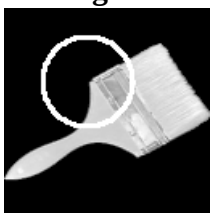


28Ff0 **28Ff0**

$$F_0(u) = \| \sum_{k=0}^{127} f(x_k) \|$$

Figure 2.2: Ring-28 to generate 28Ff0 signals.

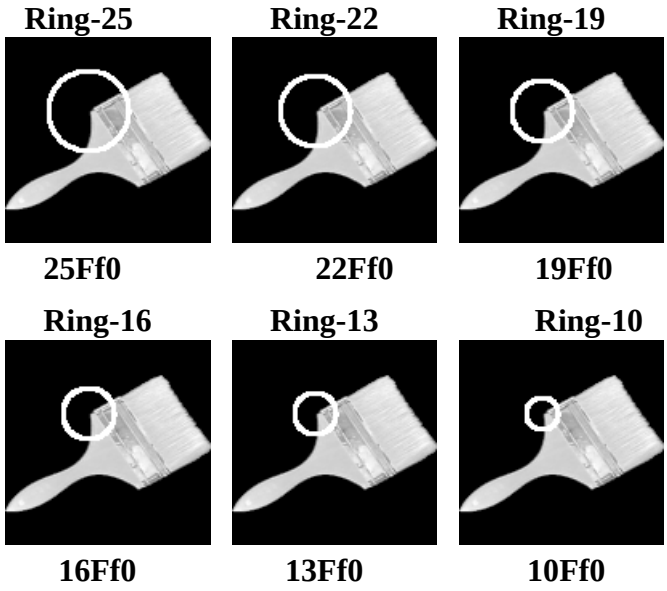

$$F_0(u) = \| \sum_{k=0}^{127} f(x_k) \|$$

Figure 2.3: Ring-25, 22, 19, 16, 13, 10 to generate 25, 22, 19, 16, 13, 10Ff0 signals.

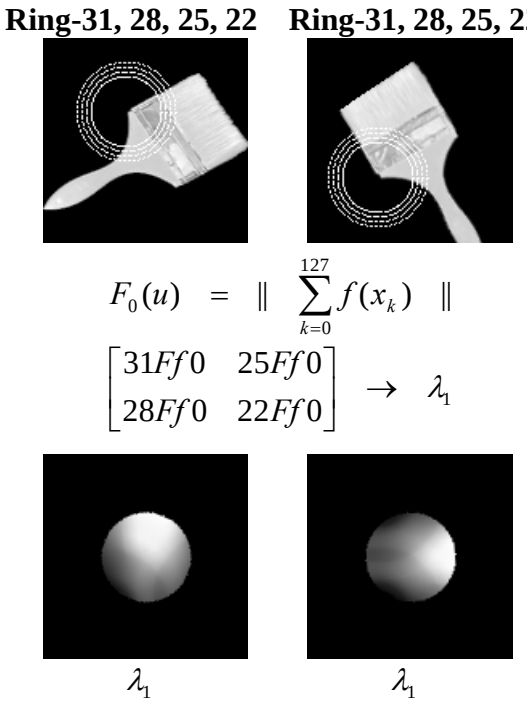

$$F_0(u) = \| \sum_{k=0}^{127} f(x_k) \|$$

$$\begin{bmatrix} 31Ff0 & 25Ff0 \\ 28Ff0 & 22Ff0 \end{bmatrix} \rightarrow \lambda_1$$

Figure 2.4: Ring-31, 28, 25, 22 to generate lambda one signals.

Ring-19, 16, 13, 10 **Ring-19, 16, 13, 10**

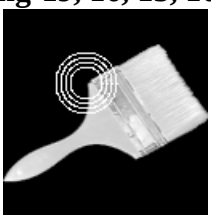


$$F_0(u) = \| \sum_{k=0}^{127} f(x_k) \|$$

$$\begin{bmatrix} 19Ff0 & 13Ff0 \\ 16Ff0 & 10Ff0 \end{bmatrix} \rightarrow \lambda_2$$

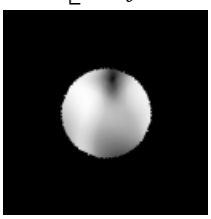
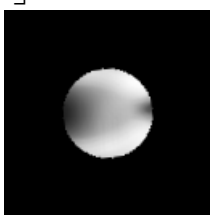

λ_2 λ_2

Figure 2.5: Ring-19, 16, 13, 10 to generate lambda two signals.

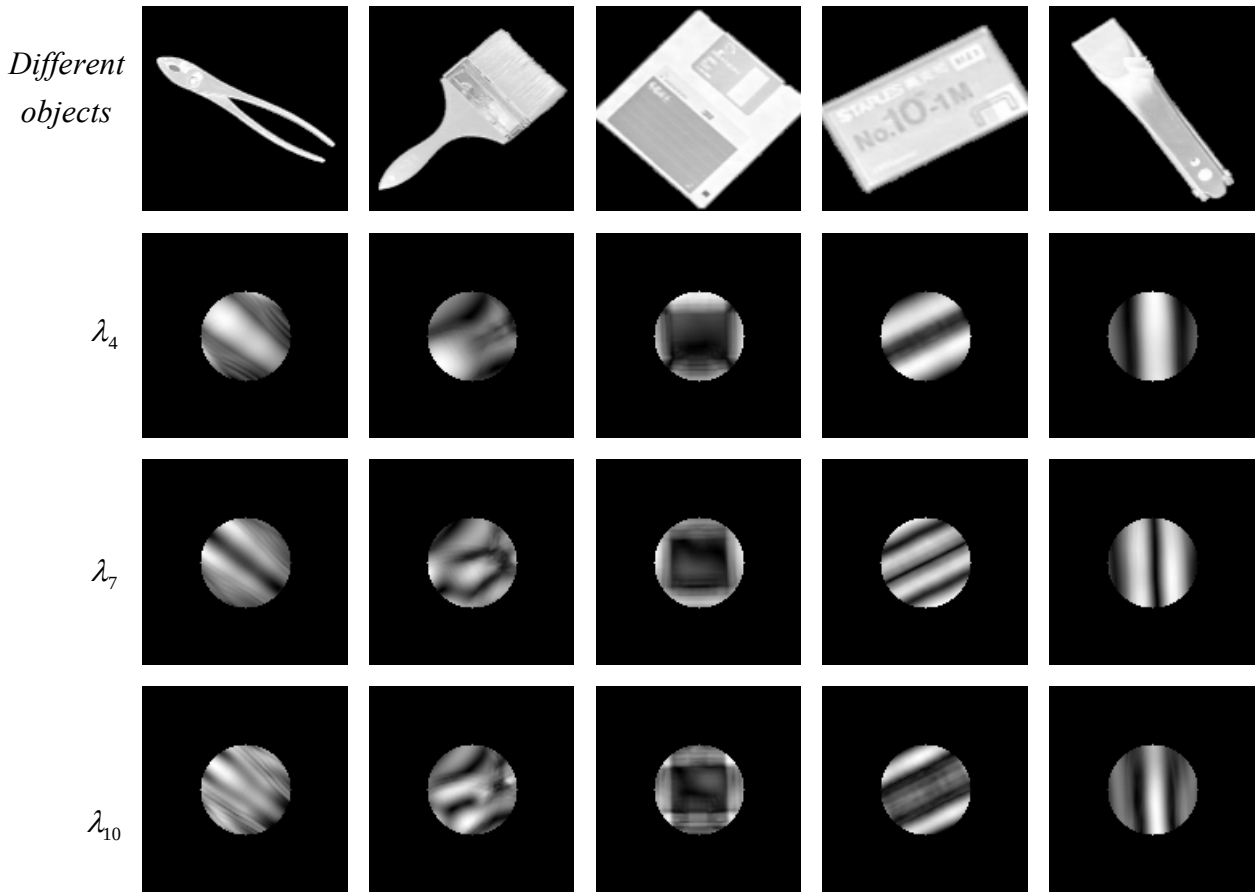

Figure 2.6: Objects and lambda signals.

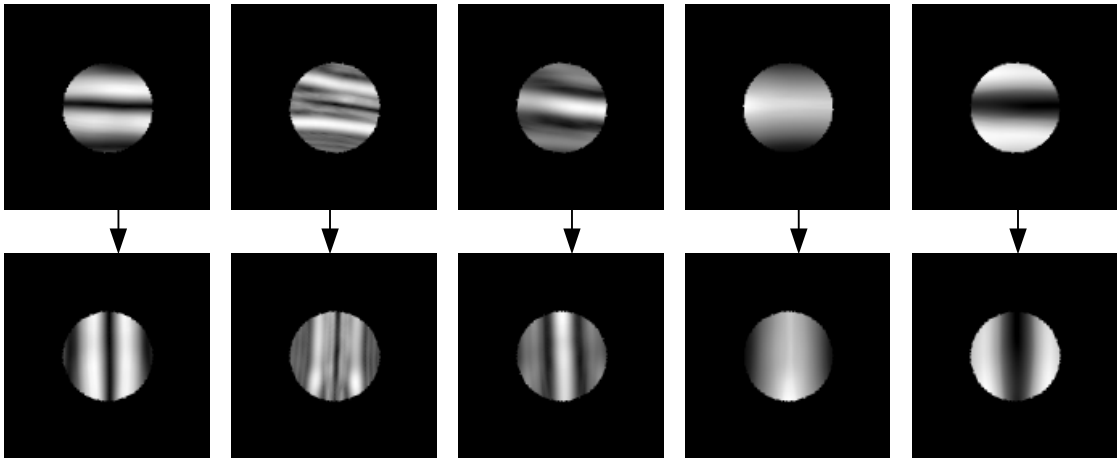

Figure 2.7: Object movement.

III. MANAGING SHIFTING PROBLEM AND COMPARING SIGNALS

The left side of figure 3.1 shows the sample image generated by the previously discussed techniques; the right side shows the unknown image, also generated as aforementioned. For managing the image-shifting problem, one pixel inside the sample image is compared with all the pixels inside the radius-6-cake search area of this unknown image. In the sample image, one specific pixel having a brighter shade of gray is located in the upper-right corner. This pixel is compared with all the pixels inside the radius-6-cake search area in the upper-right corner of the unknown image. Subsequently, the closest-matching pixel is determined. In Figure 3.2, a specific pixel located on the right side of the sample image is compared with all the pixels in the radius-6-cake search area on the right side of the unknown image in the search. Thus, the closest-matching pixel is found. The same procedure can be used for the right-bottom pixel in the left image in Figure 3.3.

The algorithm individually examines all the pixels in the sample image to compare with and search for the closest-matching pixel in the unknown image. By examining the searching results, one can judge whether the respective images are identical. Concurrently, the distance that the unknown image has shifted from the sample image can be determined.

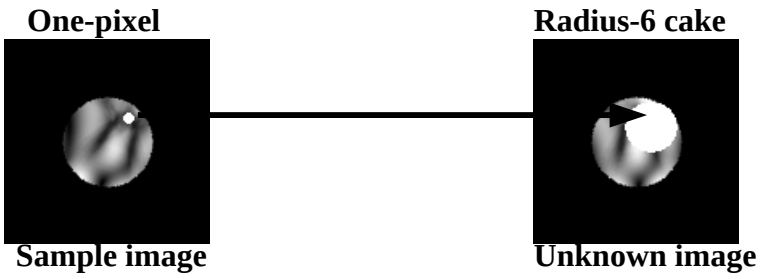

Figure 3.1: One pixel is compared with all pixels inside radius-6 cake in right image.

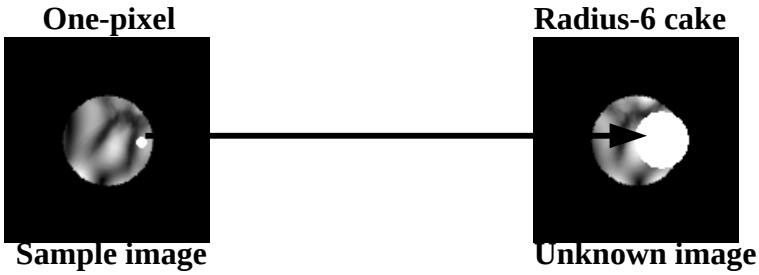

Figure 3.2: One pixel is compared with all pixels inside radius-6 cake in right image.

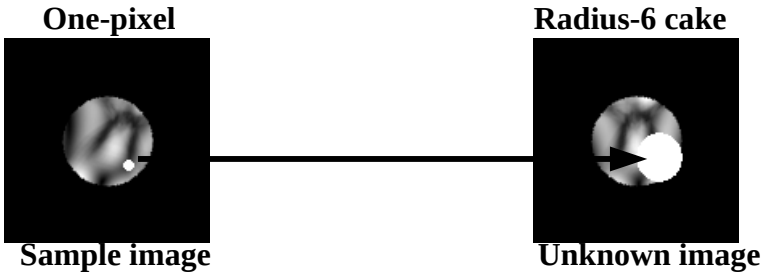

Figure 3.3: One pixel is compared with all pixels inside radius-6 cake in right image.

IV. RESULTS AND CONCLUSIONS

Figure 4.1 shows the original objects, which are used to test the accuracy in this study. In this study, each object was taken three different images. Actually, the total object images used in this system are 120, whereby regarding them as whole and running them in one batch will take a very long time to complete; moreover, due to the software glitch, the running process might break before the job completed; subsequently, the procedure might be run endlessly and every time from the beginning; furthermore, the database might have no enough memory to accommodate them; thus, in this system, objects, belonging to five objects, are designated as a batch to verify the system; since one object has been taken three different images, totally fifteen images are tested in one batch. As aforementioned, in this system, there are forty objects participating the test, to which the system totally runs eight different batches. To each batch, one object is compared with other 14 objects, by which totally 105 comparisons are conducted, whereby 15 comparisons are conducted for genuine comparisons and the other ninety imposter. In this study, one pixel in the sample image is compared with all the surrounding pixels in unknown image to locate the closest matching pixel, to which the shifting distance between the two is recorded; after examine all the pixels in sample image, the algorithm accumulates the times of each distances, by which to locate the maximum one, as recorded in table 4.1, wherein the data inside the rectangular boxes represent identical source comparisons and the others, different sources.

Figure 4.2 shows the summarized results of table 4.1, showing the gap between the imposter and genuine comparisons for five different objects. For each object the upward-pointing arrow represents the value-range of the genuine comparisons; the downward-pointing arrow, the imposter comparisons. The technique presented in this study can correctly identify the objects.

As aforementioned, the moment technique is used to align the object to the same orientation; however, glitter might present in the surface of the object “stapler” and it can not locate the correct orientation of this object; subsequently, the mal-registration results are occurred, as shown in figure 4.3. The direction of major axis of the object needed to be placed only on the upper-right and upper-left of the coordinate, i.e. the I and II quadrants; otherwise, registration error with 180 degrees occurred, as shown in figure 4.4. If the centroid algorithm cannot correctly locate the centroid of the object, various orientation errors occur, as shown in figure 4.5.

Figure 4.1: Original 128 by 128 images.

Table 4.1: Comparison data of original images.

2533	1274	37	33	40	14	13	17	31	41	66	24	26	27
	1873	37	41	44	18	9	21	27	32	48	26	24	32
		44	31	48	18	12	18	40	45	37	26	26	30
			223	60	31	34	31	34	40	40	44	61	47
				54	25	20	49	33	42	36	42	24	35
					23	17	29	17	17	21	51	33	32
						99	115	39	35	44	16	13	19
							389	33	37	43	20	14	19
								27	30	30	16	13	19
									2571	1333	43	37	56
										1600	51	34	46
											46	29	45
												253	195
													278

Comparisons of identical sources

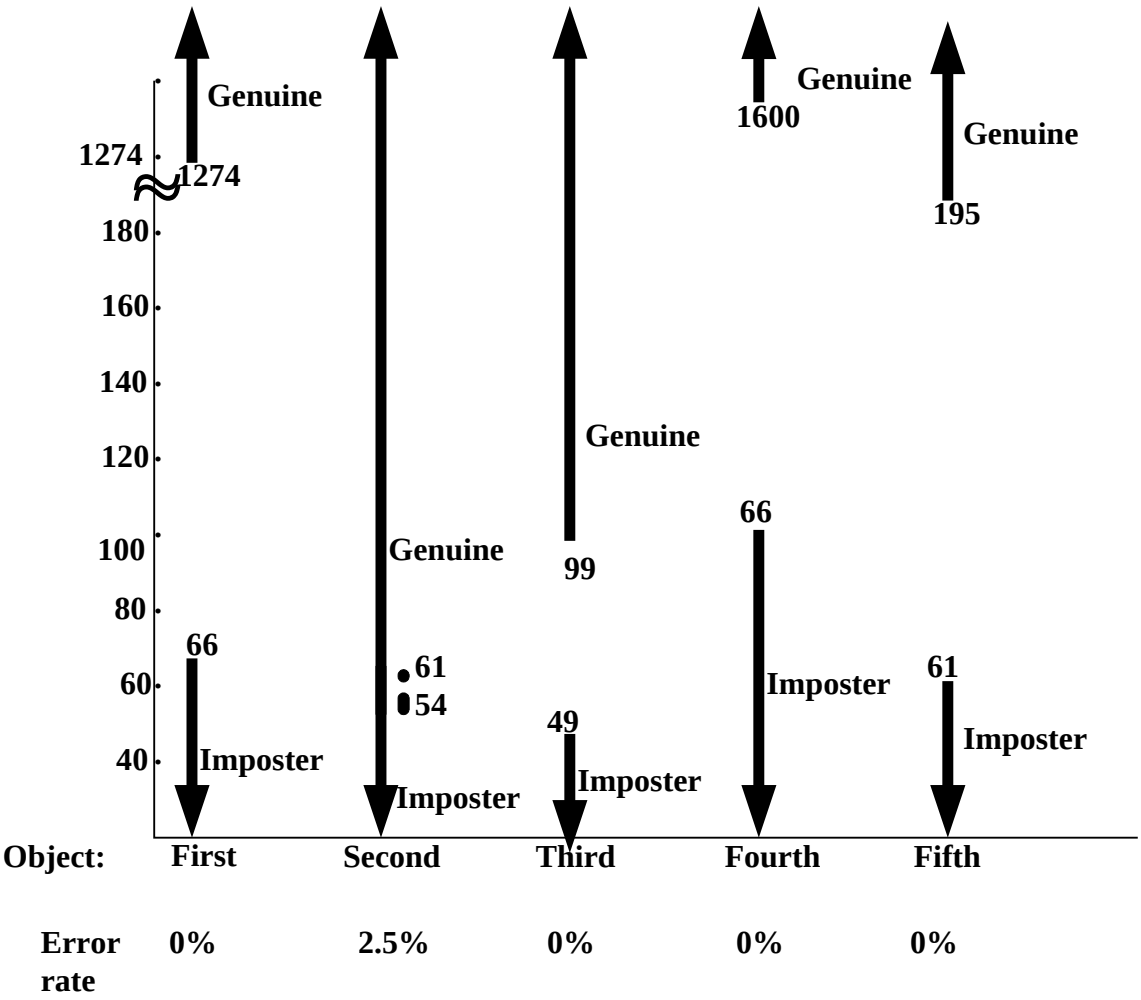

Figure 4.2: Gap between imposter and genuine comparisons.

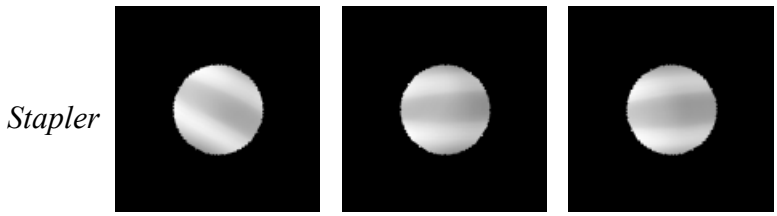

Figure 4.3: 45 degree error, stapler.

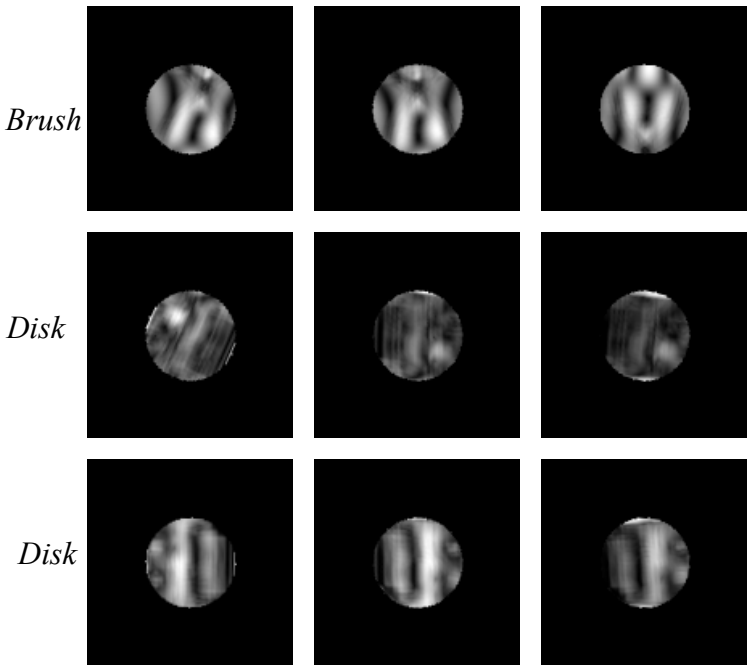

Figure 4.4: 180 degree error, brush and disk.

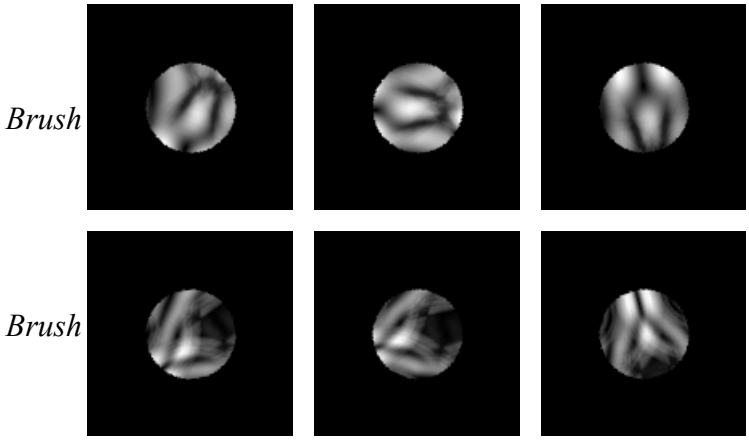

Figure 4.5: 180 and 45 degree errors, brush and disk.

REFERENCES

[1] Aditya Abhyankara, b, Stephanie Schuckersa , "A Novel Biorthogonal Wavelet Network System for Off-Angle Iris Recognition," Pattern Recognition 43 (2010) 987--1007

[2] Banafshe Arbab-Zavar and Mark S. Nixon, "On guided model-based analysis for ear biometrics," Computer Vision and Image Understanding 115 (2011) 487−502.

[3] John D. Bustard and Mark S. Nixon, Associate Member, IEEE, "Toward Unconstrained Ear RecognitionFrom Two-Dimensional Images," IEEE transactions on systems, man, and cybernetics- Part A: Systems and Humans, Vol. 40, No. 3, May 2010

[4] Craig Belcher and Yingzi Du , "Region-based SIFT approach to iris recognition," Optics and Lasers in Engineering 47 (2009) 139−147

[5] Septimiu Crisan, Ioan Gavril Tarnovan, and Titus Eduard Crisan, "Radiation optimization and image processing algorithms in the identification of hand vein patterns," Computer Standards & Interfaces 32 (2010) 130−140

[6] R. M. Farouk, "Iris recognition based on elastic graph matching and Gabor wavelets," Computer Vision and Image Understanding 115 (2011) 1239−1244

[7] Miguel A. Ferrer and Aythami Morales, "Hand-Shape Biometrics Combining the Visible and Short-Wave Infrared Bands," IEEE transactions on information forensics and security, vol. 6, no. 4, December 2011

[8] Cong Geng and Xudong Jiang, "Face Recognition Based on the Multi-Scale Local Image Structures," Pattern Recognition 44 (2011) 2565−2575

[9] Ajay Kumar and Chenye Wu, "Automated Human Identification Using Ear Imaging," Pattern Recognition 45 (2012) 956–968

[10] Karen Hollingsworth, Kevin W. Bowyer, and Patrick J. Flynn, "Pupil dilation degrades iris biometric performance," Computer vision and image understanding 113 (2009) 150−157

[11] Haifeng Hu, "Multiscale illumination normalization for face recognition using dual-tree complex wavelet transform in logarithm domain," Computer vision and image understanding 115 (2011) 1384−1394

[12] Deng-Yuan Huang, Wu-Chih Hu, and Sung-Hsiang Chang, "Gabor filter-based hand-pose angle estimation for hand gesture recognition

under varying illumination," Expert Systems with Applications 38 (2011) 6031−6042

[13] Hong Huang, JiaminLiu, Hailiang Feng, and Tongdi He, "Ear Recognition Based on Uncorrelated Local Fisher Discriminant Analysis ," Neurocomputing 74 (2011) 3103−3113

[14] Vivek Kanhangad, Ajay Kumar, and David Zhang, "A Unified Framework for Contactless Hand Verification," IEEE transactions on information forensics and security, vol. 6, no. 3, September 2011

[15] Antonio Iula and Michele De Santis, "Experimental evaluation of an ultrasound technique for the biometric recognition of human hand anatomic elements," Ultrasonics 51 (2011) 683−688

[16] Amirhosein Nabatchian, Esam Abdel-Raheem, and Majid Ahmadi, "Illumination invariant feature extraction and mutual-local matching for face recognition under illumination variation and occlusion," Pattern Recognition 44 (2011) 2576−2587

[17] Yingbo Zhou and Ajay Kumar, "Human Identification Using Palm-Vein Images," IEEE transactions on information forensics and security, vol. 6, no. 4, December 2011